Coupling light to periodic nanostructures

Driessen, E.F.C.

CHAPTER 7

Observation of coupling between surface plasmons in index-matched hole arrays

We measured the transmission of a large array of holes in an optically thick gold film, immersed in liquids of different refractive index. For a large difference in refractive index between the substrate and the liquid ($\Delta n \gtrsim 0.05$), the transmission spectra contain separate resonances, due to coupling to surface plasmons propagating on each of the metal-to-dielectric interfaces. When the index difference is reduced, we observe an avoided crossing between a strong low-energy mode and a weak high-energy mode. The low-energy mode becomes broader and gains amplitude at the expense of the high-energy mode. For an index-matched array, a single broad resonance remains. These observations provide direct evidence that the two surface-plasmon modes on different sides of the interface are coupled.

7.1 Introduction

It is well known that coupling of different surface plasmon modes on the same interface, via Bragg scattering, leads to the formation of bright and dark modes in 1-D arrays of slits or wires [54, 65, 66]. Alternatively, plasmons on a single interface can be coupled to a waveguide mode [67, 68]. The coupling between plasmons on different interfaces is more difficult to observe, because in most cases the plasmon resonances on different sides of the metal film are detuned in frequency. This is due to the inherent asymmetry of a metal film on a substrate. This asymmetry can be removed by either fabricating a symmetric sample or by using index matching liquids [69–71]. The observed transmission spectra generally resemble the calculated spectra [70, 72], but the finite size of the arrays and the numerical aperture of the incoming beam limit a proper observation of the coupling between the modes.

Here, we present transmission measurements on a large two-dimensional metal hole array, using a white light beam with a numerical aperture that is small enough to resolve the coupled modes. We obtain the frequency, the linewidth, and the amplitude of the resonances by fitting multiple Fano resonances to the transmission spectra [53, 54]. When the index difference between substrate and liquid is reduced we observe an avoided crossing between a broad low-energy mode and a narrow high-energy mode. At the same time, the linewidth and the amplitude of the low-energy mode increase at the expense of the high-energy mode. These modes correspond to the two peaks in the transmission spectrum, which can be identified as surface plasmons propagating on either the substrate or the liquid side of the metal film. Our observations can be described by a coupled-mode theory, and are consistent with calculations that use tunneling of light through the holes as the coupling mechanism [70, 72].

7.2 Experiments

For our experiments, we mounted a metal hole array on a glass substrate inside a closed glass cuvette with a 2.5 mm optical path length. The array was immersed in different refractive-index solutions. We used mixtures of ethanol and benzyl alcohol to cover the range $n=1.36$–1.54 and mixtures of benzyl alcohol and bromo-naphtalene for the range $n=1.54$–1.66. The refractive index of each mixture was determined by Abbe refractometry, and is close to the volume average of the refractive index of the two liquids. The glass substrate (Schott-BK7) has a nearly constant refractive index $n=1.51$ over the wavelength range of interest. The metal hole array is a large (1×1 mm^2) square

array of 200 nm diameter holes with a lattice constant $a = 700$ nm, in an optically thick (200 nm) gold film. A 2 nm thick Ti bonding layer ensures proper adhesion of the gold layer. The optical transmission was measured at normal incidence. We used a fiber-coupled lamp to illuminate a $\sim 300~\mu$m diameter spot on the sample, thus avoiding edge effects. The transmitted light was sent to a fiber-coupled grating spectrometer with a Si CCD array (resolution 1.2 nm, 550-1000 nm) or an InGaAs linear array (resolution 3.0 nm, 900-1700 nm). Apertures in the incident and transmitted light beam were used to limit the numerical aperture below 0.01.
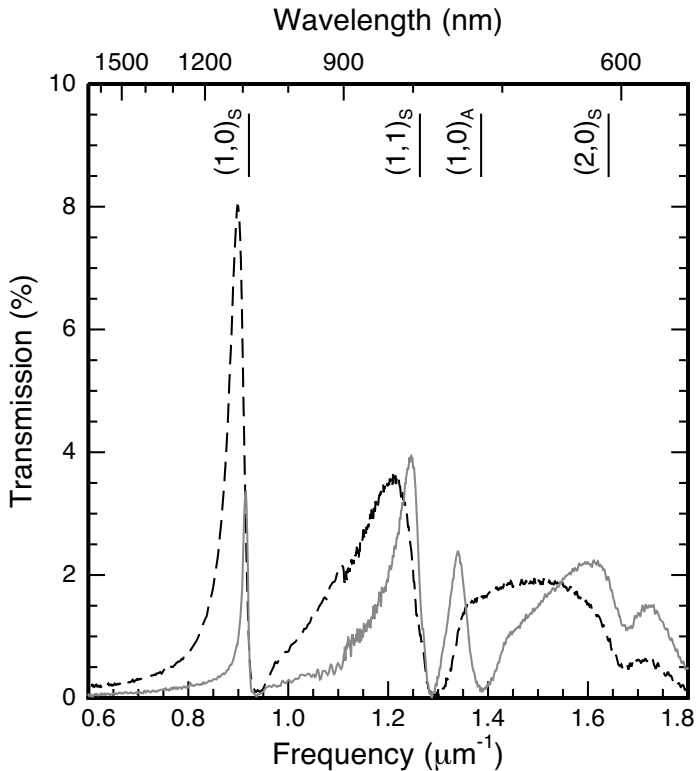
Figure 7.1. Transmission as function of frequency for a metal hole array in air (solid curve, $n_L = 1.00$) and nearly index matched (dashed curve, $n_L = 1.50$). The vertical lines indicate the calculated spectral positions of the different plasmon resonances on the substrate (S) and air (A) side of the array for $n_L = 1.00$.

Figure 7.1 shows the measured transmission as function of frequency. Spectra are shown for the metal hole array in air (solid line), and immersed in a
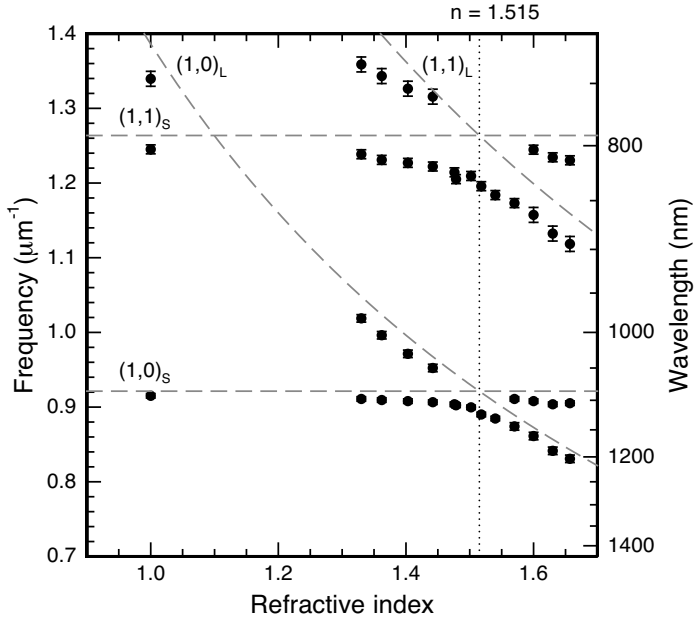
Figure 7.2. Frequencies of the maximum in transmission as a function of the refractive index obtained directly from the transmission data. The dashed curves show the calculated resonance frequencies according to Eq.(7.1).

liquid with refractive index $n_{\mathrm{L}} = 1.50$ (dashed curve). The spectra show a number of resonant peaks for which the transmission is enhanced. This is a result of coupling of incident radiation to surface plasmons that propagate on either the metal-to-air or the metal-to-substrate interface. The condition for coupling to such a surface plasmon is given by $\vec{k}_{\parallel} = \vec{k}_{\mathrm{SP}} + \vec{G}$, where $\vec{k}_{\parallel}$ is the component of the wave vector of the incident light along the interface, $\vec{k}_{\mathrm{SP}}$ is the wave vector of the surface plasmon and $\vec{G}$ is a reciprocal lattice vector. For normal incidence this condition leads to a set of resonance frequencies given by

$$\omega_{\mathrm{res}} = \frac{|\vec{G}|c}{n}\sqrt{1 + \frac{n^2}{\epsilon_{\mathrm{m}}(\omega)}}, \qquad (7.1)$$

where c is the speed of light in vacuum, n is the refractive index of the dielectric, and $\epsilon_m(\omega)$ is the frequency-dependent dielectric constant of the metal. For a square lattice, the length of the reciprocal lattice vector is $|\vec{G}| = \sqrt{(N_{\mathrm{x}}^2 + N_{\mathrm{y}}^2)}2\pi/a$, with N_{x} and N_{y} integer. Therefore, the resonances

can be labelled as $(N_x, N_y)_{S,A}$, where the subscript indicates whether the resonance occurs on the substrate (S) or on the air (A) side of the metal hole array. To calculate the resonance frequencies we use literature values of the dielectric constant of gold [60] and take the dielectric constants of air and glass as constant. The vertical lines in Fig. 7.1 indicate the calculated positions of the different resonances. For an asymmetric structure with air on one side and glass on the other side, the resonances from the two sides are well separated.

When the air is replaced by a nearly index-matching liquid, the transmission spectrum changes drastically (dashed curve in Fig. 7.1). The $(1,0)_A$ mode on the metal-to-liquid interface shifts in frequency from 1.387 μm^{-1} (721 nm) to 0.922 μm^{-1} (1085 nm) to coincide with the $(1,0)_S$ mode on the metal-to-substrate interface. The peak transmission of the combined $(1,0)$ mode is roughly a factor of two higher, and a significant broadening of the resonance is observed.

The frequencies of the maxima in the transmission spectra are plotted in Fig. 7.2 as a function of the refractive index of the liquid (symbols). The dashed lines are the frequencies of the different modes as predicted by Eq. (7.1). The modes can be classified in two categories: modes on the metal-to-substrate interface (labelled 'S'), which do not shift when the index of the liquid is changed, and modes on the metal-to-liquid interface (labelled 'L'), which show a strong red-shift in frequency when the refractive index of the liquid is increased. To correctly predict the resonance frequencies from Eq. (7.1) the frequency dependent dielectric constant of the metal should be included. The index dispersion of the liquids and the glass can be neglected.

7.3   Model

The transmission through a metal hole array can be described as a combination of a non-resonant direct transmission through the holes, and a resonant component that couples to surface plasmons [53, 54, 72–74]. Interference between these two contributions gives an asymmetric line shape. The transmission spectra $T(\omega) = |t(\omega)|^2$ can be expressed as a sum over a finite number of (uncoupled) resonances

$$t(\omega) = a_{nr}\omega^2 + \sum_j \frac{b_j \Gamma_j \exp(i\varphi_j)}{(\omega - \omega_j) + i(\Gamma_j + \gamma_j)}, \qquad (7.2)$$

where Γ_j is the radiative loss and γ_j is the intrinsic Ohmic loss of mode j. The resonance at frequency ω_j has an amplitude b_j and a phase φ_j. The slowly varying non-resonant contribution has an amplitude a_{nr} and is proportional
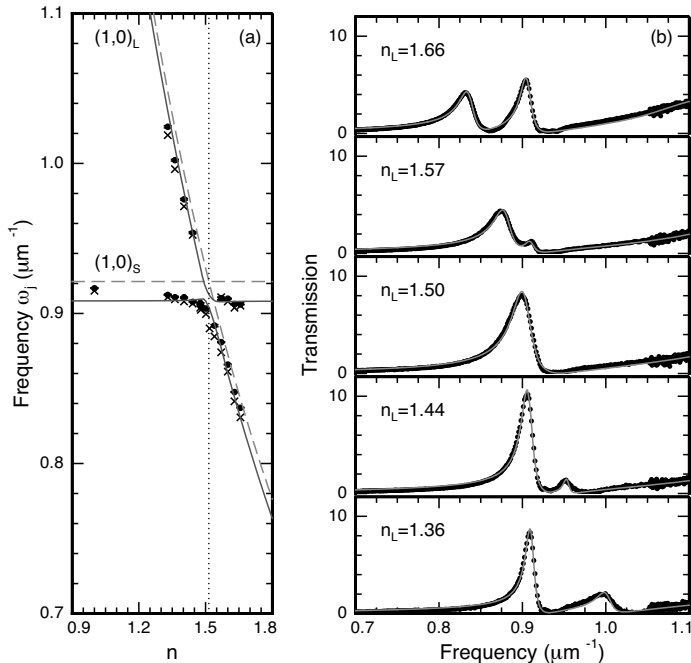
Figure 7.3. Detail of the crossing between the (1,0) modes (a) and corresponding spectra (b). The crosses are the peak frequencies obtained directly from the measured data, while closed symbols are the frequencies ω_j from fitting the transmission data to 4 Fano resonances. The solid curves are a fit to coupled-mode theory (see text). The dashed lines are the calculated frequencies for the uncoupled surface-plasmon resonances. The measured transmission (b) is shown for different refractive indices of the liquid (dots) and can be fitted to the Fano expression (curves)

to ω^2 to reflect the fact that the transmitted intensity through a single sub-wavelength hole is proportional to ω^4 for a single, sub-wavelength hole in a thin film of a perfect conductor [51]. In the limit of long wavelengths, the dielectric constant of the metal approaches that of the perfect conductor, while the film thickness relative to the wavelength becomes negligible and Eq. 7.2 gives the correct result. In principle, Eq. (7.2) allows a separation of resonant and non-resonant contributions, but in practice the number of separate resonances that can be identified in measured transmission spectra is limited. This complicates the interpretation of a_{nr} because the non-resonant term now also contains a contribution from resonances at higher frequencies.

Figure 7.3 shows the frequency of the peaks as a function of the refractive

index in more detail (a), and corresponding transmission measurements in the frequency range between 0.7 and 1.1 μm^{-1} (b). The solid curves are fits of Eq. (7.2), containing up to 4 resonant contributions. In these fits, the Ohmic losses γ_j were set to zero*. This description is valid for the typical situation that the radiative loss is much larger than the intrinsic Ohmic loss. The number of fit parameters can be reduced by setting all phases φ_j equal to π. This corresponds to the normal situation, where the resonant channel is out of phase with the direct channel. This choice does not affect the values of the other fit parameters significantly.

The crosses in Fig. 7.3(a) indicate the frequencies of the transmission maxima determined directly from the experimental data. These maxima are close to the resonance frequencies obtained from the fits (solid symbols). When the refractive index of the liquid is close to that of the substrate, the transmission spectrum is reduced to a single peak. Two distinct peaks can be observed for an index difference between liquid and substrate larger than ∼0.05. In addition, the linewidth and amplitude of the resonances depend strongly on the refractive index. The low-frequency resonance broadens and grows in amplitude when the refractive index is increased, while the high-frequency resonance narrows and diminishes in amplitude.

Figure 7.4 shows the linewidth Γ_j and square amplitude b_j^2 obtained from the fit of Eq. (7.2) to the transmission data. The triangular symbols refer to a fit where all parameters were kept free, while the circular symbols refer to a fit with all phases φ_j equal to π. The data in Fig. 7.4 confirm that the low-frequency mode (mode 1) gains amplitude and broadens while the high-frequency mode (mode 2) is reduced in amplitude and narrows. Note that a typical value of $\Gamma = 0.01$ μm^{-1} corresponds to a propagation distance $x = 1/(2\pi\Gamma) \approx 16$ μm. This is much smaller than the illuminated spot size (300 μm) and the coherence length $D \approx \lambda/\text{NA}$, which we estimate > 100 μm for a NA of less than 0.01. The avoided crossing together with the data in Fig. 7.4 prove that the two surface plasmons on different sides of the optically thick metal film are coupled.

A coupled-mode theory with only 2 modes is sufficient to describe our data. These modes correspond to the two surface plasmons that propagate on either the substrate or the liquid side of the metal film. In this analysis, we treat the plasmon modes on the same interface that are coupled via Bragg reflection [54, 65, 66] as a single mode. The time evolution of the amplitudes a

---

*The parameters b_j, Γ_j and γ_j are not independent and cannot be determined by a fit of the data to Eq. (7.2).
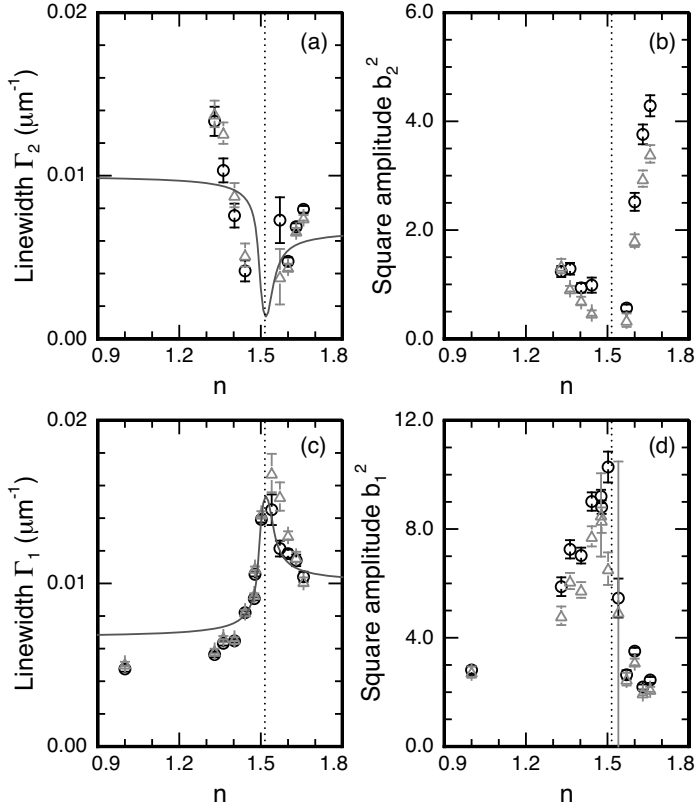
Figure 7.4. Linewidth Γ and square amplitude b^2 for the lowest two resonances as function of refractive index. The low-frequency mode (c,d) is always present and both linewidth and amplitude show a maximum around the index matched situation ($n_{\rm L} = 1.515$, dotted line). At the same time, the second mode shows a minimum in linewidth and amplitude and disappears from the spectra for nearly index-matched samples. The solid curve is a fit to coupled-mode theory (see text).

and b of the two modes in our model is given by the equation of motion

$$i\frac{\mathrm{d}}{\mathrm{d}t}\left(\begin{array}{c} a \\ b \end{array} \right) = H\left(\begin{array}{c} a \\ b \end{array} \right).\tag{7.3}$$

The Hamiltonian H that describes the coupled system has the following form:

$$H = \left(\begin{array}{cc} \omega_{\rm a} + V - i\Gamma_{\rm a} & W + i\Gamma_{\rm C} \\ W + i\Gamma_{\rm C} & \omega_{\rm b} + V - i\Gamma_{\rm b} \end{array} \right).\tag{7.4}$$

Table 7.1. Fit parameters of the coupled-mode theory described in the text

V	: Frequency shift	-0.013	$\pm$	0.028	μm^{-1}
Γ_a	: Damping rate of mode a	0.0067	$\pm$	0.0004	μm^{-1}
Γ_b	: Damping rate of mode b	0.0100	$\pm$	0.0005	μm^{-1}
W	: Conservative coupling rate	0.0046	$\pm$	0.0015	μm^{-1}
Γ_C	: Dissipative coupling rate	0.0068	$\pm$	0.0011	μm^{-1}

The diagonal elements of the matrix contain the frequencies $\omega_{a,b}$ and linewidths $\Gamma_{a,b}$ of the uncoupled modes, and a frequency shift V. The off-diagonal elements contain parameters W and Γ_C that describe conservative coupling (leading to mode splitting and an avoided crossing), and dissipative coupling (leading to mode pulling or frequency locking), respectively [75, 76]. The complex eigenvalues of the Hamiltonian H give the frequencies $\omega_{1,2}$ and linewidths $\Gamma_{1,2}$ of the coupled modes.

The solid curves in Figs. 7.3(a) and 7.4 are a fit of the model to the experimental data[*]. The fit parameters are summarized in Table 7.1. There is a small frequency red-shift V, compared to the resonance frequencies predicted by Eq. (7.1), which is consistent with the theory in Ref. [72]. The conservative coupling rate W causes the avoided crossing in Fig. 7.3(a). The frequencies ω_j can be fit satisfactorily by setting the dissipative coupling rate Γ_C to zero. However, a system with only conservative coupling gives line widths $\Gamma_{1,2}$ that are independent of refractive index. This is inconsistent with the data in Fig. 7.4. To describe the fact that the line width of one mode increases while the line width of the other mode decreases, a dissipative component in the coupling is needed. Conservative coupling is still important because a model with only dissipative coupling ($W = 0$) gives significant mode pulling, which is not observed in our measurements. As a comparison, Fig. 7.5 shows the fitted line widths for coupled mode theories with only conservative coupling (a), only dissipative coupling (b), and both conservative and dissipative coupling (c).

As a refinement of our model, we have also used damping rates $\Gamma_{a,b}$ that depend on the refractive index of the liquid via the optical density of states [54, 77, 78]. Introducing these extra fit parameters indeed results in a better fit. However, it does not affect the values of the fit parameters V, W and Γ_C significantly, and thus does not change our interpretation of the measurements. The fit parameters in table 7.1 indicate that the mode on the liquid side is

---

[*]The fit was obtained by fitting the frequency and linewidth data simultaneously, giving equal weight to each of the points.
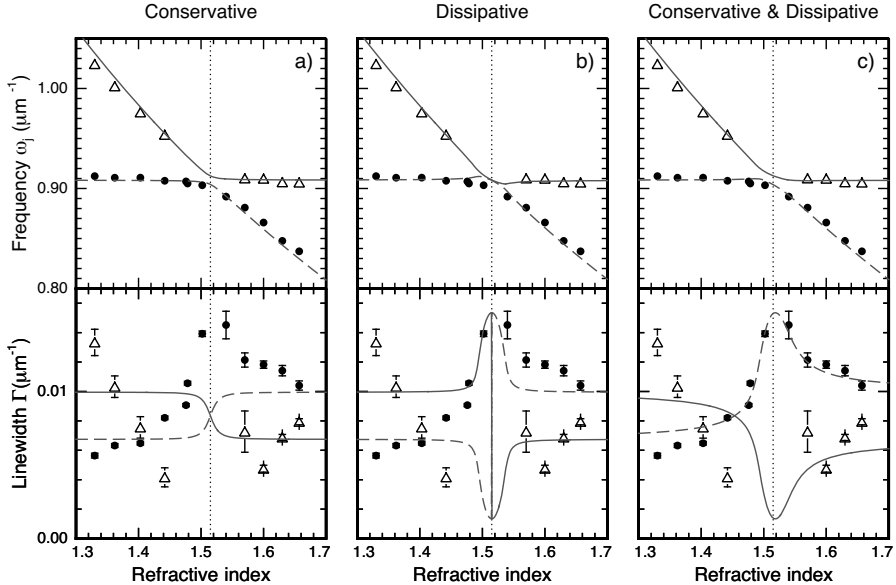
Figure 7.5. Frequencies and linewidths of the $(1,0)$ resonance as function of the refractive index of the liquid. The values are obtained from a Fano fit of the measured transmission spectra at normal incidence and compared to coupled mode theory with only conservative coupling (a), only dissipative coupling (b) or both conservative and dissipative coupling (c). The closed symbols (data) and dashed curves (theory) indicate the low-energy mode, while the open triangles and solid curves indicate the high-energy mode.

somewhat more lossy than the mode on the glass side. It is reasonable to assume that this is due to the fact that the roughness of the metal-to-liquid interface is larger than the interface between the metal and the polished glass substrate. From AFM measurements on the sample, we indeed find roughness (rms) values of 4.4 nm for the gold surface, and 0.8 nm for the glass surface. In addition, some residual particles from the fabrication process are present on the gold-air interface, which will add to the scattering of surface plasmons on this interface.

The modes in our coupled-mode theory are consistent with the states calculated using a scattering formalism [70, 72]. On resonance, the eigenmodes correspond to a situation where the plasmons on the two interfaces oscillate in phase (low-frequency mode) or out of phase (high-frequency mode). Close to resonance, the calculated spectra show a split resonance (avoided crossing) and a linewidth of the low-energy mode that becomes larger, while the linewidth

of the high-energy mode becomes smaller. Without absorption the amplitude of the modes is equal. If absorption is included, the amplitude of the peaks is reduced depending on the linewidth (resonance time) of the mode [70]. This explains the dependence of the squared amplitude $b_{1,2}^2$ of the modes as function of refractive index given in Fig. 7.4.

7.4   Conclusion

In conclusion, an experiment where surface-plasmon resonances on either side of a metal hole array are tuned into degeneracy, gives insight into the coupling between these surface-plasmon modes. Two plasmon modes, on different sides of the metal film, can be identified if there is a large mismatch in refractive index. The resonance in the transmission spectra is reduced to a single broad resonance when the sample is index matched. This behavior can be explained by a coupling between the two surface plasmon modes through the hole-array. A coupled-mode analysis shows that the modes have an avoided crossing and correctly predicts the change in linewidth of the coupled modes when the refractive index is changed.